Journal of Thermal Analysis and Calorimetry
https://doi.org/10.1007/s10973-024-13134-3

Computational analysis of power-law fluids for convective heat transfer in permeable enclosures using Darcy effects

Maryam Rehman[1] · **Muhammad Bilal Hafeez**[2] · **Marek Krawczuk**[2]

Received: 26 November 2023 / Accepted: 31 March 2024

Abstract

Natural convection is a complex environmental phenomenon that typically occurs in engineering settings in porous structures. Shear thinning or shear thickening fluids are characteristics of power-law fluids, which are non-Newtonian in nature and find wide-ranging uses in various industrial processes. Non-Newtonian fluid flow in porous media is a difficult problem with important consequences for energy systems and heat transfer. In this paper, convective heat transmission in permeable enclosures will be thoroughly examined. The main goal is to comprehend the intricate interaction between the buoyancy-induced convection intensity, the porosity of the casing, and the fluid's power-law rheology as indicated by the Rayleigh number. The objective is to comprehend the underlying mechanisms and identify the ideal conditions for improving heat transfer processes.The problem's governing equations for a scientific investigation are predicated on the concepts of heat transport and fluid dynamics. The fluid flow and thermal behavior are represented using the energy equation, the Boussinesq approximation, and the Navier–Stokes equations. The continuity equation in a porous media represents the conservation of mass. Finite Element Analysis is the numerical method that is suggested for this challenging topic since it enables a comprehensive examination of the situation. The results of the investigation support several important conclusions. The power-law index directly impacts heat transmission patterns. A higher Rayleigh number indicates increased buoyancy-induced convection, which increases the heat transfer rates inside the shell. The porosity of the medium significantly affects temperature gradients and flow distribution, and it is most noticeable when permeability is present. The findings show how, in the context of porous media, these parameters have complicated relationships with one another.

Keywords Numerical study · Darcy effect · Heat Transfer · Permeable dynamics · Finite element method

List of symbols

u, v	Velocity components
ρ	Fluid density
p	Fluid pressure
g	Gravity
α	Thermal diffusivity
β	Thermal expansion coefficient
T	Fluid temperature
n	Power-law index
Da	Darcy parameter
Ra	Rayleigh number
Pr	Prandtl number
K.E.	Kinetic energy

✉ Muhammad Bilal Hafeez
Muhammad.bilal.hafeez@pg.edu.pl

[1] Department of Mathematics, Air University, P.A.F Complex E-9, Islamabad 44000, Pakistan

[2] Faculty of Mechanical Engineering and Ship Technology, Institute of Mechanics and Machine Design, Gdansk University of Technology, Narutowicza 11/12, 80-233 Gdańsk, Poland

Introduction

The phenomenon of natural convection heat transfer is an important part of engineering and industry, finding extensive application in various fields like nuclear energy [1, 2] and electronics [3–6]. For Cooling, solar energy, geophysics, and other industrial systems spanning numerous industries. The low thermal conductivity of conventional fluids, such as a mixture of water, oil, and ethylene glycol, is a major obstacle to improving heat transmission in these engineering systems. Studies in [7, 8] investigated the effects of eccentricity and Rayleigh number on heat transfer through natural convection in a fluid enclosed by two horizontal isothermal cylinders and nanofluids. It is crucial to fill enclosures with

Published online: 30 April 2024

materials that have extensive properties. Before the introduction of the non-Newtonian fluid rheology idea, many of the cavities were filled with air and water. As material testing equipment has advanced, non-Newtonian fluid. In that fluids that challenge the laws of motion of viscosity rules are now routinely recommended due to their significant practical value in industrial and mechanical processes. In an industrial setting, non-Newtonian fluid analysis is more significant due to the nonlinear dependency of stress and strain, but it still requires particular study. The analysis of non-Newtonian fluids in enclosures is essential to many industries, such as nuclear reactors, food processing, oil drilling, polymer manufacturing, geophysical systems, and electronic cooling systems. Ozoe and Churchill [9] might have been the first to demonstrate the hydrodynamic properties of a power-law fluid in a shallow horizontal cavity by examining the recirculation produced in the fluid flow zone. In their study, the authors of [10] use a finite difference method to simulate Rayleigh-Bénard convection of dependent power-law fluids in a square cavity. The cavity was heated from the bottom and cooled from the top with uniform heat fluxes. Their aim was to investigate the two-dimensional stable state of the system. The transient flow of a power-law fluid in a vertical cavity and the concurrent heat transfer from natural convection were studied by Kim et al. in their study [11]. The author of [12] uses both numerical and experimental approaches to study the steady-state natural convective fluid flow and heat transfer in a vertical rectangular enclosure partially filled with a vertical layer of fluid-saturated porous media. The influence of surface waviness on natural convective heat transfer from an isothermal surface in a porous Darcian fluid-saturated enclosure was quantitatively investigated in [13] using the finite element method on a stepped non-uniform mesh system. The natural convective heat transfer in a cavity with a porous media and a wall of sinusoidal vertical waves is studied numerically. In [14], the vertical walls are isothermal; while, the horizontal straight walls are still adiabatic. The significance of the heated/cooled walls' thermal boundary conditions for heat transfer and entropy generation inside a porous enclosure that is heated from below is examined by the author in [15]. Using nonlinear thermal radiation, modified heat and mass fluxes, slip condition, and the Cattaneo–Christov heat flux model applied to a Riga plate, [16] performs a mathematical analysis of a three-dimensional Eyring–Powell nanofluid. It presents comparisons between bvp4c results and shooting technique with graphical and numerical illustrations of key parameters. Considering both symmetric and asymmetric conduit configurations in physiological models, [17] presents a novel mathematical analysis of Cilia propulsion for a non-Newtonian Couple Stress fluid with electroosmosis and heat transfer. It provides exact solutions, graphical illustrations, and a thorough comparison study that highlights higher flow values, pressure rise, and pressure gradient in asymmetric conduits. To improve heat transfer, decrease entropy generation, and reconcile the theoretical model with experimental results, [18] examines engine oil-based hybrid nanofluid flow past a nonlinearly stretching surface. It does this by presenting a comparative study on slip conditions, using a variable magnetic field, and validating results using a modified homotopy analysis approach. It also shows that entropy in engine oil flow can be optimized with specific nanoparticle concentrations. Using ternary nanomaterials under the shape parameters of nanoparticles, [19] suggests a novel way to increase the efficiency of annular fins in natural convection, to improve their performance for systems such as injector pumps, thermal engineering, and electronics.

Significance of the project

Because of the novel connections made in this work, no prior research on the issue of natural convective heat transfer involving a power-law fluid in a permeable enclosure has been done. The process involves defining the problem, mathematical modeling, mesh generation, boundary conditions, material property specification for the power-law fluid, post-processing for data analysis, validating results, and potentially executing sensitivity analyses and optimization in order to solve the governing equations using the FEA technique. With the use of sophisticated FEA software, the objective is to comprehend and optimize heat transfer inside the enclosure simulations. The research has been split into five categories as a result, each of which offers a range of potential fixes. The details of the current problem are presented in Part 2. Meanwhile, the numerical method is summarized in Section "Results and Discussion". Sect. "Comparison of heat transfer between different geometries" discusses the findings. This study is concluded in Sect. "Conclusions".

Assumptions of the current problem

The assumptions and requirements for the mathematical model are as follows:

- Heat transfer rate
- Isothermal boundaries
- Homogeneous and Isotropic Material properties
- Prandtl number approximation
- Darcy number and Permeability
- Boussinesq approximation

Mathematical model

This model deals with the exciting relationship between heat transfer and fluid dynamics when power-law fluids are present in a porous enclosure. Assume that a time-independent, laminar power-law flow is saturated within a pyramid, like a triangular enclosure. The applicability of our problem is further illustrated by the placement of a cold obstacle in the triangle's center, which has a radius of 0.05. All the boundaries are non-slip, even though the top wall and the other walls are not heated uniformly. For this problem, the Finite Element Method is the most efficient numerical method. The main reason for choosing the Finite Element Method (FEM) for this extensive analysis is that it can effectively simulate intricate structures with non-uniform geometries and diverse material compositions. FEM is an excellent tool for precisely solving a wide range of engineering issues, including fluid dynamics, thermal, and structural assessments. It is a chosen numerical technique because of its ability to handle dynamic scenarios, adjust to real-world settings, and achieve precision through mesh refinement. As a flexible and potent tool for a broad range of engineering simulations, FEM effectively handles complex geometries and material heterogeneity, in contrast to certain other approaches. By representing the density included in the buoyancy term and accounting for the role of natural convection in the flow regime, the Boussinesq approximation keeps all physical quantities at rest. A physical diagram of the issue is presented in Fig. 1.

The governing equations listed below offer a solid foundation for examining the intricate physics at play. A full understanding of the system behavior is provided by the dimensional and non-dimensional parameters, such as the Rayleigh number (Ra), Prandtl number (Pr), and Darcy number (Da).

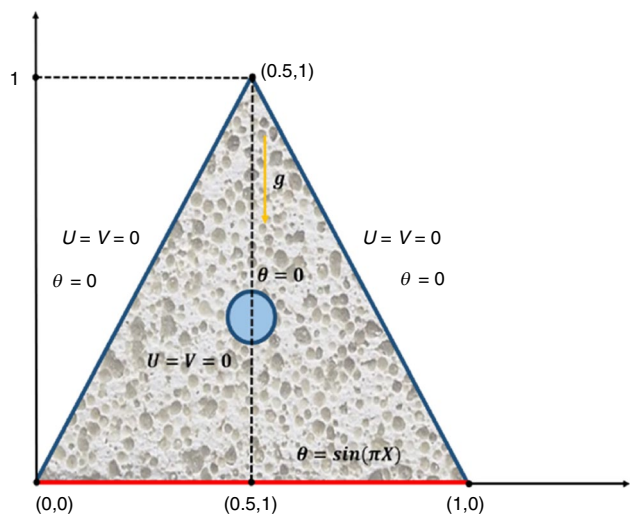

Fig. 1 Geometry of the problem

The dimensional form of governing equations of the problem are as follows:

$$\frac{\partial u}{\partial x}+\frac{\partial v}{\partial y}=0, \tag{1}$$

$$\rho\left(u\frac{\partial u}{\partial x}+v\frac{\partial u}{\partial y}\right)=-\frac{\partial p}{\partial x}+\frac{\partial}{\partial x}\left(2\mu_{\mathrm{a}}\left(\frac{\partial u}{\partial x}\right)\right)+\frac{\partial}{\partial y}\left(\mu_{\mathrm{a}}\left(\frac{\partial v}{\partial x}+\frac{\partial u}{\partial y}\right)\right)-\frac{\mu}{k_{\mathrm{m}}}u, \tag{2}$$

$$\rho\left(u\frac{\partial v}{\partial x}+v\frac{\partial v}{\partial y}\right)=-\frac{\partial p}{\partial y}+\frac{\partial}{\partial x}\left(\mu_{\mathrm{a}}\left(\frac{\partial v}{\partial x}+\frac{\partial u}{\partial y}\right)\right)+\frac{\partial}{\partial y}\left(2\mu_{\mathrm{a}}\left(\frac{\partial v}{\partial y}\right)\right)+g\rho\beta(T-T_{\mathrm{c}})-\frac{\mu}{k_{\mathrm{m}}}v, \tag{3}$$

$$u\frac{\partial T}{\partial x}+v\frac{\partial T}{\partial y}=\alpha\left(\frac{\partial^2 T}{\partial x^2}+\frac{\partial^2 T}{\partial y^2}\right). \tag{4}$$

The transformations used for non-dimensionalization of the governing equations are:

$X=\frac{x}{L}, Y=\frac{y}{L}, U=\frac{uL}{\alpha}, V=\frac{vL}{\alpha}, P=\frac{pL^2}{\rho\alpha^2}, \theta=\frac{T-T_{\mathrm{c}}}{\Delta T}, \Delta=\frac{qL}{k},$

The non-dimensionalized form of governing equations of the problem are as follows:

$$\frac{\partial U}{\partial X}+\frac{\partial V}{\partial Y}=0, \tag{5}$$

$$\left(U\frac{\partial U}{\partial X}+V\frac{\partial U}{\partial Y}\right)=-\frac{\partial P}{\partial X}+\mathrm{Pr}\left[2\frac{\partial}{\partial X}\left\{\mu_{\mathrm{a}}^{*}\frac{\partial U}{\partial X}\right\}+\frac{\partial}{\partial Y}\left\{\mu_{\mathrm{a}}^{*}\left(\frac{\partial V}{\partial X}+\frac{\partial U}{\partial Y}\right)\right\}\right]-\frac{\mathrm{Pr}}{\mathrm{Da}U}, \tag{6}$$

$$\left(U\frac{\partial V}{\partial X}+V\frac{\partial V}{\partial Y}\right)=-\frac{\partial P}{\partial Y}+\mathrm{Pr}\left[\frac{\partial}{\partial X}\left\{\mu_{\mathrm{a}}^{*}\left(\frac{\partial V}{\partial X}+\frac{\partial U}{\partial Y}\right)\right\}+2\frac{\partial}{\partial Y}\left\{\mu_{\mathrm{a}}^{*}\frac{\partial V}{\partial Y}\right\}\right]-\frac{\mathrm{Pr}}{\mathrm{Da}\,\mathrm{Pr}\,\theta} \tag{7}$$

$$U\frac{\partial\theta}{\partial X}+V\frac{\partial\theta}{\partial Y}=\frac{\partial^2\theta}{\partial X^2}+\frac{\partial^2\theta}{\partial Y^2}. \tag{8}$$

The dimensional form of boundary conditions are as follows: $u(x,0)=0=v(X,0),\ T(X,0)=T_{\mathrm{k}}-T_{\mathrm{c}}$ or $fu(x,y)=0=v(x,y), T=T_{\mathrm{c}}$ at $x=y$ and $0\le x\le 0.5,\ 0\le y\le L$, $u(x,y)=0=v(x,y), T=T_{\mathrm{c}}$ at $L-x=y$ and $0.5\le x\le L, 0\le y\le L$, $u=v=T=0$, for cold cylinder.

The non-dimensionalized form of boundary conditions are as follows:

$U(X,0)=0=V(X,0),\ \theta(X,0)=\sin(\pi x)$, and $0\le X\le 1$,

$U(X,Y) = 0 = V(X,Y),\ \theta = 0 \text{at} X = Y \text{and} 0 \le X, Y \le 0.5$,

$U(X,Y) = 0 = V(X,Y), \theta = 0$ at $1 - X = Y$ and $0 \le Y \le 0.5,\ 0.5 \le X \le 1$,

$U = V = \theta = 0$, for the cold cylinder.

Dimensional Apparent Viscosity:

$$\mu_a = k\left[2\left(\left(\frac{\partial u}{\partial x}\right)^2 + \left(\frac{\partial v}{\partial y}\right)^2\right) + \left(\frac{\partial v}{\partial x} + \frac{\partial u}{\partial y}\right)^2\right]^{\frac{n-1}{2}}. \quad (9)$$

where μ_a, which is previously defined as the apparent dimensionless viscosity, is used.

Dimensionless Apparent Viscosity:

$$\mu_a^* = \left[2\left(\left(\frac{\partial U}{\partial X}\right)^2 + \left(\frac{\partial V}{\partial Y}\right)^2\right) + \left(\frac{\partial V}{\partial X} + \frac{\partial U}{\partial Y}\right)^2\right]^{\frac{n-1}{2}}. \quad (10)$$

Dimensionless Parameters:
$\text{Ra} = \frac{g\beta\Delta TL^{2n+1}}{k\alpha^n}$, $\text{Pr} = \frac{kL^{2n-2}}{\rho\alpha^{2-n}}$, $\text{Da} = \frac{k_m}{L^2}$

Results and discussion

This model's practical importance stems from its immediate uses and promising future developments. Solving this problem has immediate benefits and practical ramifications for many different domains. The study's conclusions may open the door to novel technologies, better procedures, or deeper comprehension, presenting encouraging opportunities for developments in linked fields and influencing the course of upcoming studies and applications.

Table 1 [16]. Variation in degrees of freedom and no. of elements at different refinement levels

Refinement level	Number of elements	Degrees of freedom
Extremely Coarse	220	2025
Extra Coarse	412	3553
Coarser	609	5096
Coarse	1183	9387
Normal	1547	12,103

Meshing

Figure 2a–b display different levels of refinement that illustrates the discretization of the fluid flow domain. As can be seen, triangular and quadratic elements make up the discretization, and $P_2 - P_1$ elements are indulged.

Table 1 shows the degree of freedom and element distribution in the three-sided domain at various enhancement levels. Discretization of the domain is a primary technique for obtaining results with the FEM scheme. The refinement levels are displayed in this tabulation from extremely coarse to extremely fine, showing that boundary and domain elements increase as refinement levels rise.

Velocity and temperature profiles

The outcomes of the calculation for the thermal and velocity profiles in a power-law fluid are shown below.

Figure 3a–c use streamlines and velocity plots against various power-law index (n) magnitudes for showing how the velocity patterns change. Figure 3a shows the fluid flow behavior against with finer mesh the power-law index (n) in

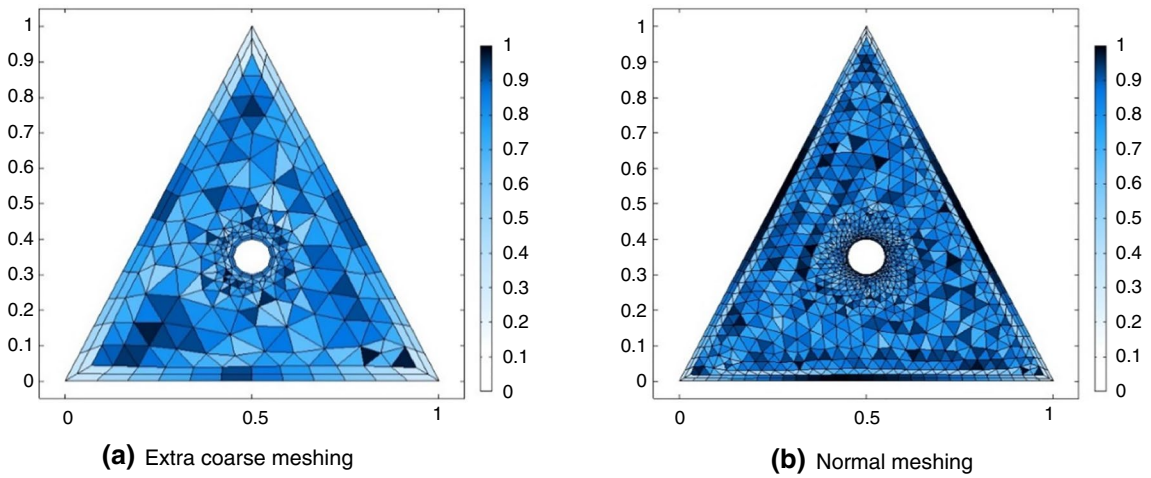

Fig. 2 Representation of extra coarse and normal refinement levels of the structure

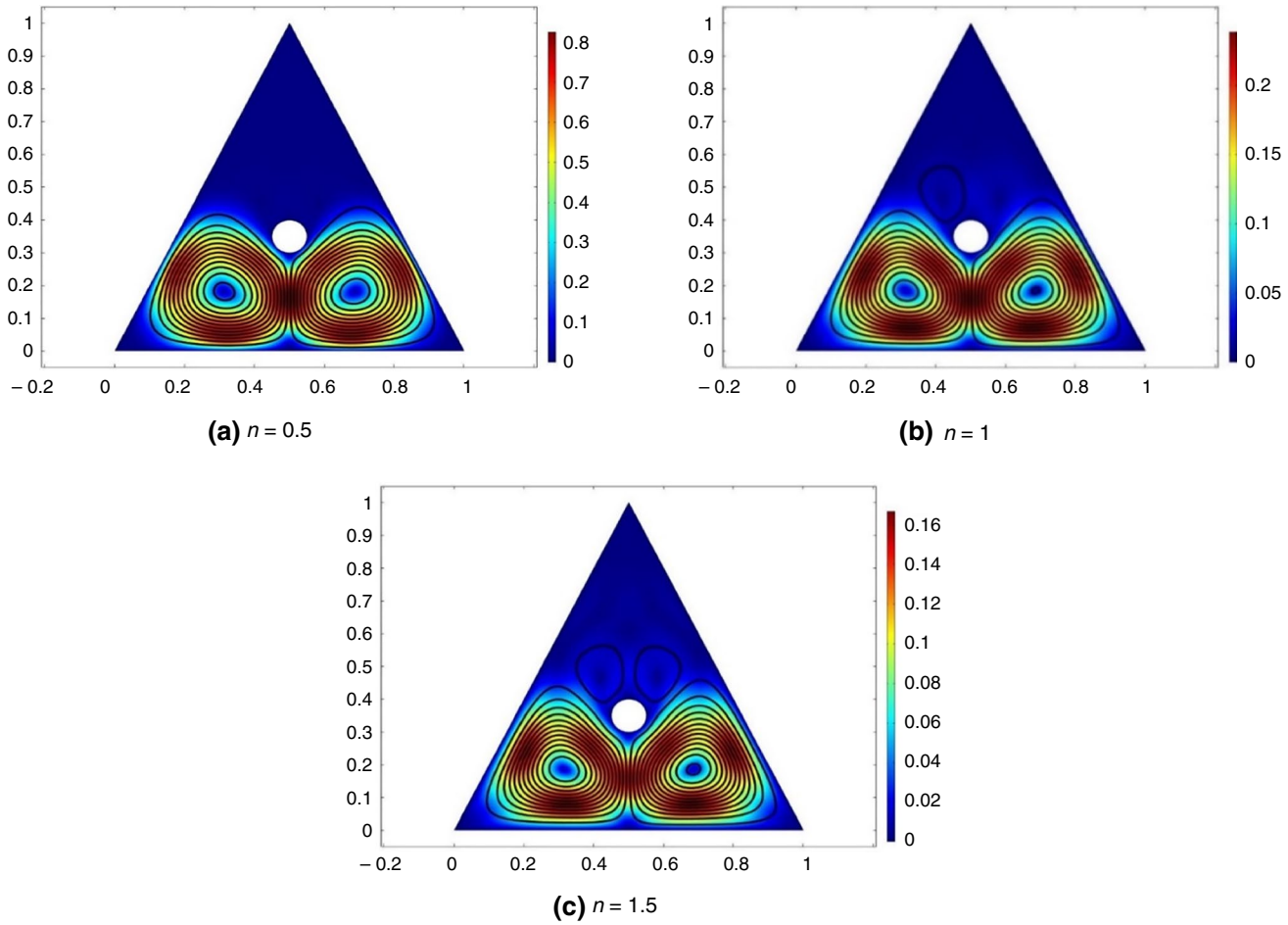

Fig. 3 Discrepancy in velocity distribution against (n) at Da = 0.00001

the shear thinning case ($n = 0.5$), where the circular flow pattern is determined. The power-law fluid shear thinning behavior is represented by the fixed $n = 0.5$ in this figure, which causes the viscosity magnitude to be minute and the fluid particles to diffuse in the shape of a circle while moving faster. However, for $n = 1$ and $n = 1.5$, the deformation in the Momentum profile pattern is interpreted. Refer to figs. (3a–3c).

Figure 4a–c shows the momentum circulation against the Rayleigh number (Ra). The flow rate shows a noticeable variation as (Ra) increases with finer meshing. This phenomenon is caused by a temperature gradient that is created in the flow field as the Rayleigh number (Ra) increases, producing buoyancy forces. These resilient forces cause the particles to disperse more, which in consequently causes a flow.

Figure 5a–c, shows velocity plots and streamlines that display how the velocity distribution varies in relation to the Darcy number (Da) under a constant Rayleigh number (Ra) with finer mwshing. Above figures represent the fluid velocities under various Darcy number conditions. Whereas the velocity plots present the extent and direction of the fluid velocity at various points, the streamlines display the paths followed by the fluid particles. A better understanding of the characteristics of heat transfer and fluid dynamics at values of Ra can be obtained by analyzing the properties of Darcy number on the current patterns and velocities of the system.

From the displayed sketches in Fig. 6a–c, sharpness in the temperature profile can be obtained by increasing (Ra). As the non-uniform heating is now changing as a function of $\theta = \mathrm{Sin}(\pi x)$, parabolic shape isothermal curves are first obtained at $\mathrm{Ra} = 10^3$, and parabolic heat formation is then achieved by growing the magnitude of (Ra). The fact that (Ra) increases the inertial forces between fluid particles, which are dependent on changes in temperature, further demonstrates the increase in heat transport with (Ra).

Figure 7a–d provides an interpretation of the temperature distribution variation with respect to Prandtl number (Pr) with finer meshing. Temperature increases are noted in relation to exceeding magnitudes of (Pr). Since the momentum to viscous diffusion rates ratio is known as the Prandtl number (Pr). Therefore, as (Pr) increases, fluid particle kinetic

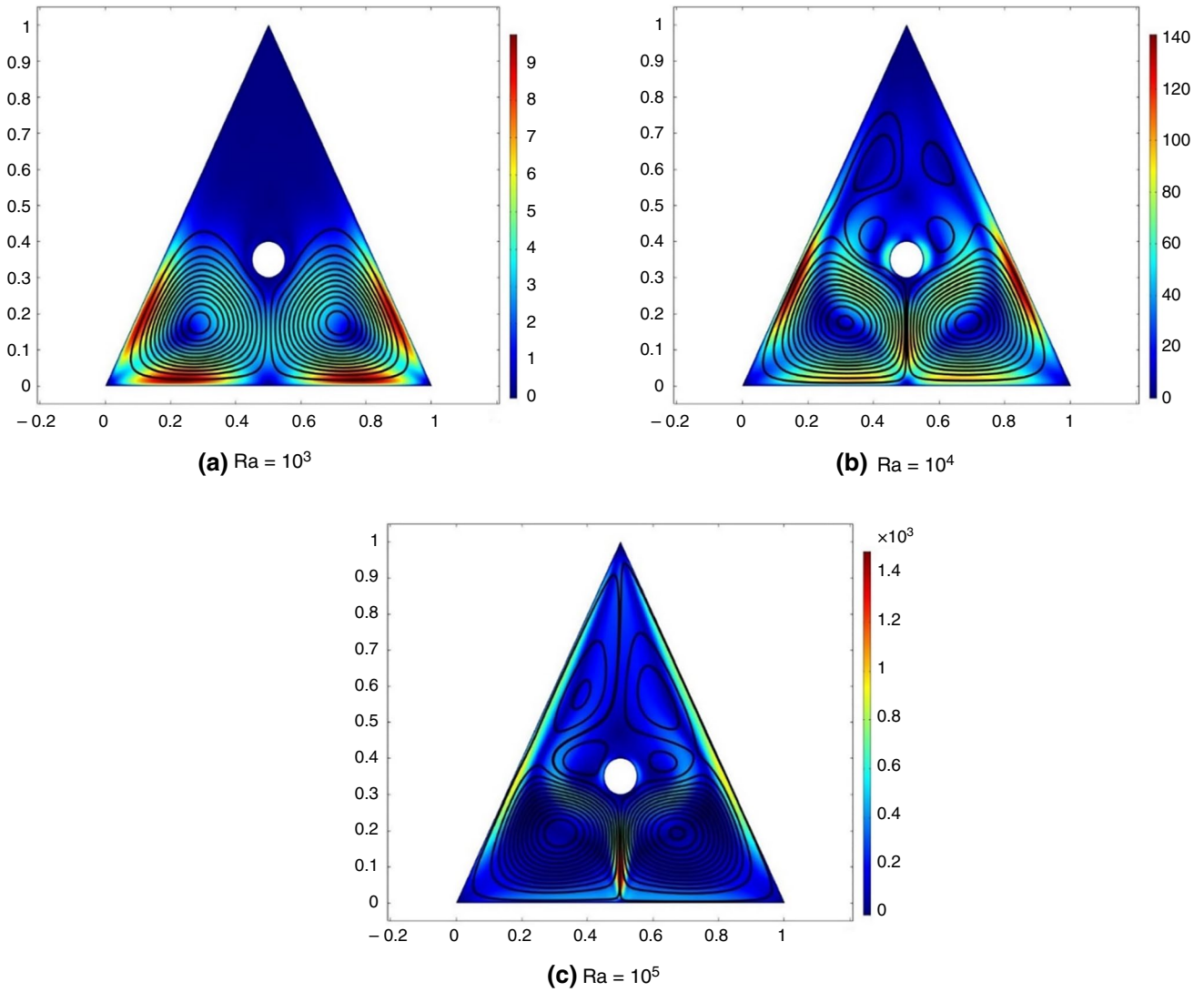

Fig. 4 Variation in velocity distribution against (Ra) at Da = 0.00001

energy rises and diffusivity increases. The temperature of fluid particles rises as a result of this increase in kinetic energy (K.E), and heat energy diffuses swiftly.

Table graphs

Table 2. and Fig. 8. depict the disparity of kinetic energy against various extents of (n) ranging from $0.5 \leq n \leq 1.5$. In this case, $n < 1$ specifies a shear thinning case, $n = 1$ indicates a Newtonian case, and $n > 1$ indicates a shear thickening case. The data illustrates that shear thinning fluid has a larger magnitude of (K.E) than Newtonian and shear thickening fluids. A decrease in kinetic energy is observed as (n) increases due to an increase in fluid viscosity and a change in the fluid mode from shear thinning to thickening behavior. There is consequently a reduction in (K.E) and less molecular movement.

Table 3. And Fig. 9. Illustrate how the Rayleigh number (Ra) affects the K.E. of particles in the flow region. Three distinct cavity locations are taken into consideration in the figure: $x = 0.3$, close to the cavity's left corner; $x = 0.5$, which is in the center of the base; and $x = 0.8$, which is at the base's right corner. The sketch suggests that as (Ra) increases, (K.E) rises as well. This fact is explained by the fact that as (Ra) increases, momentum is created in the fluid flow and inertial forces overpower viscous forces. Kinetic energy rises sequentially (Table 4).

Table 5 shows how changes in the Rayleigh number (Ra), Prandtl number (Pr), and Darcy number (Da) affect the Nusselt number (Nu). the data shows different value for Ra, Pr, Da, and the related Nusselt number. The Nusselt

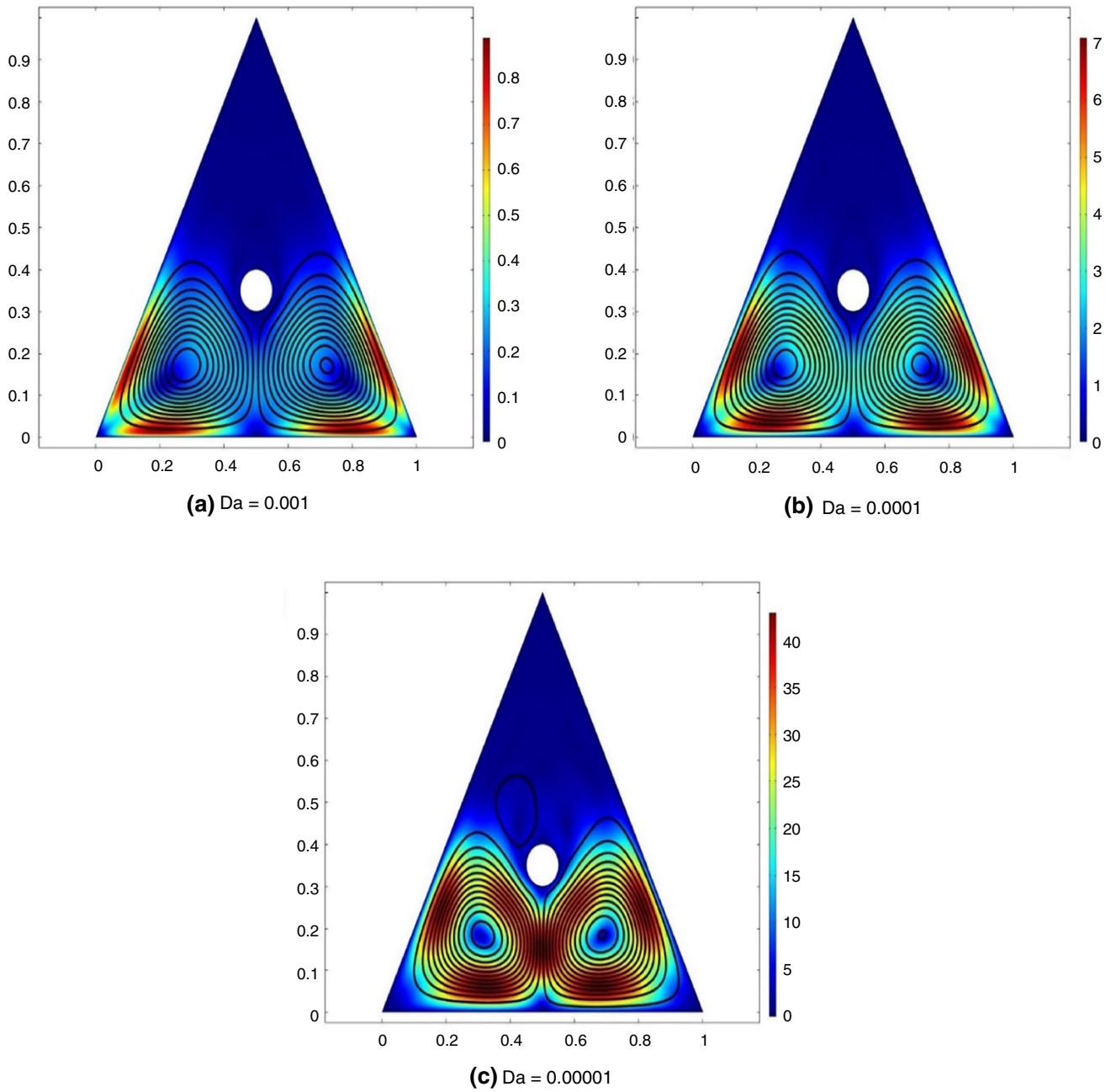

Fig. 5 Variation in velocity distribution against (Da) at Ra = 1000

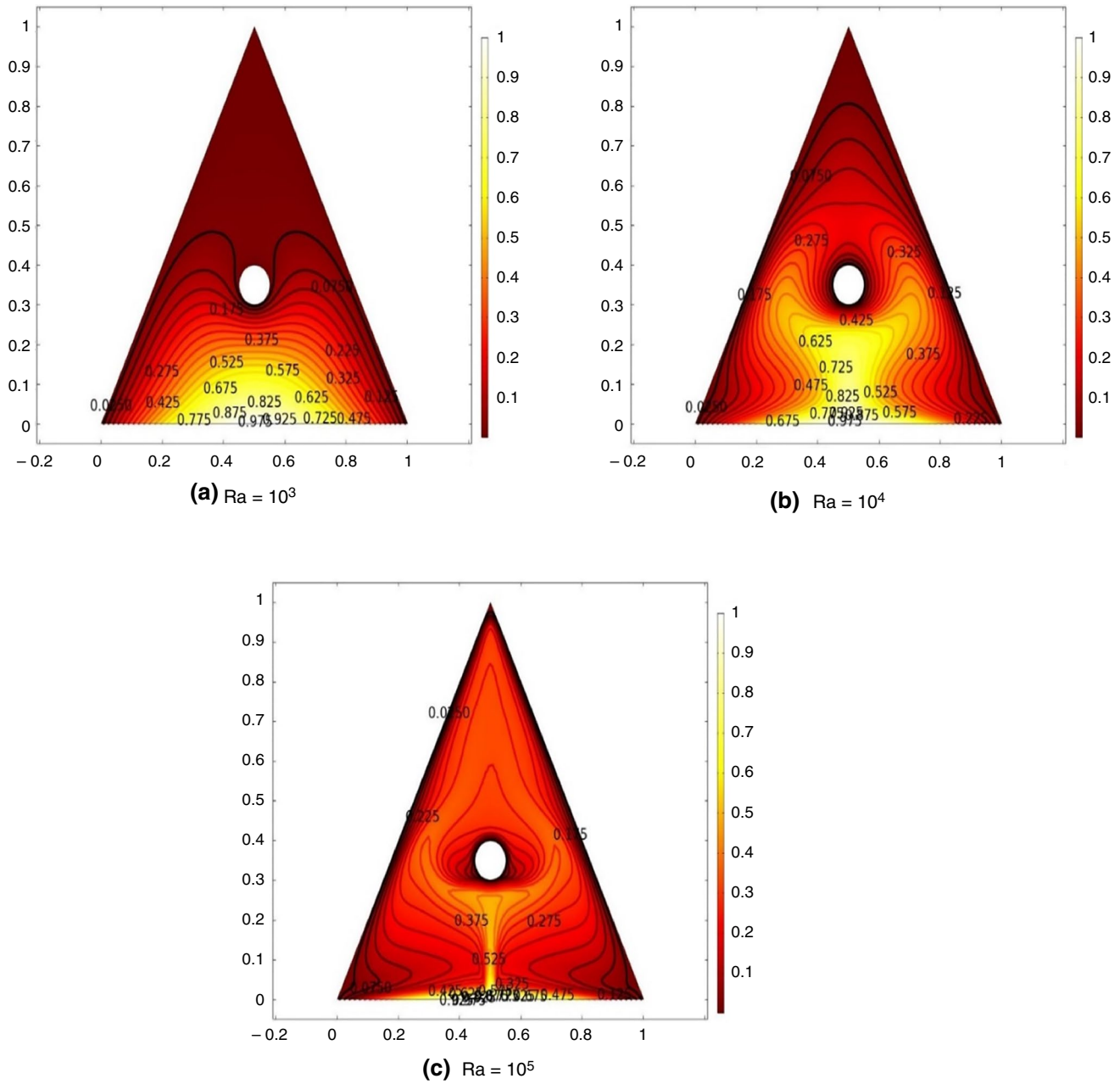

Fig. 6 Variation in thermal profile against (Ra) at Da = 0.00001

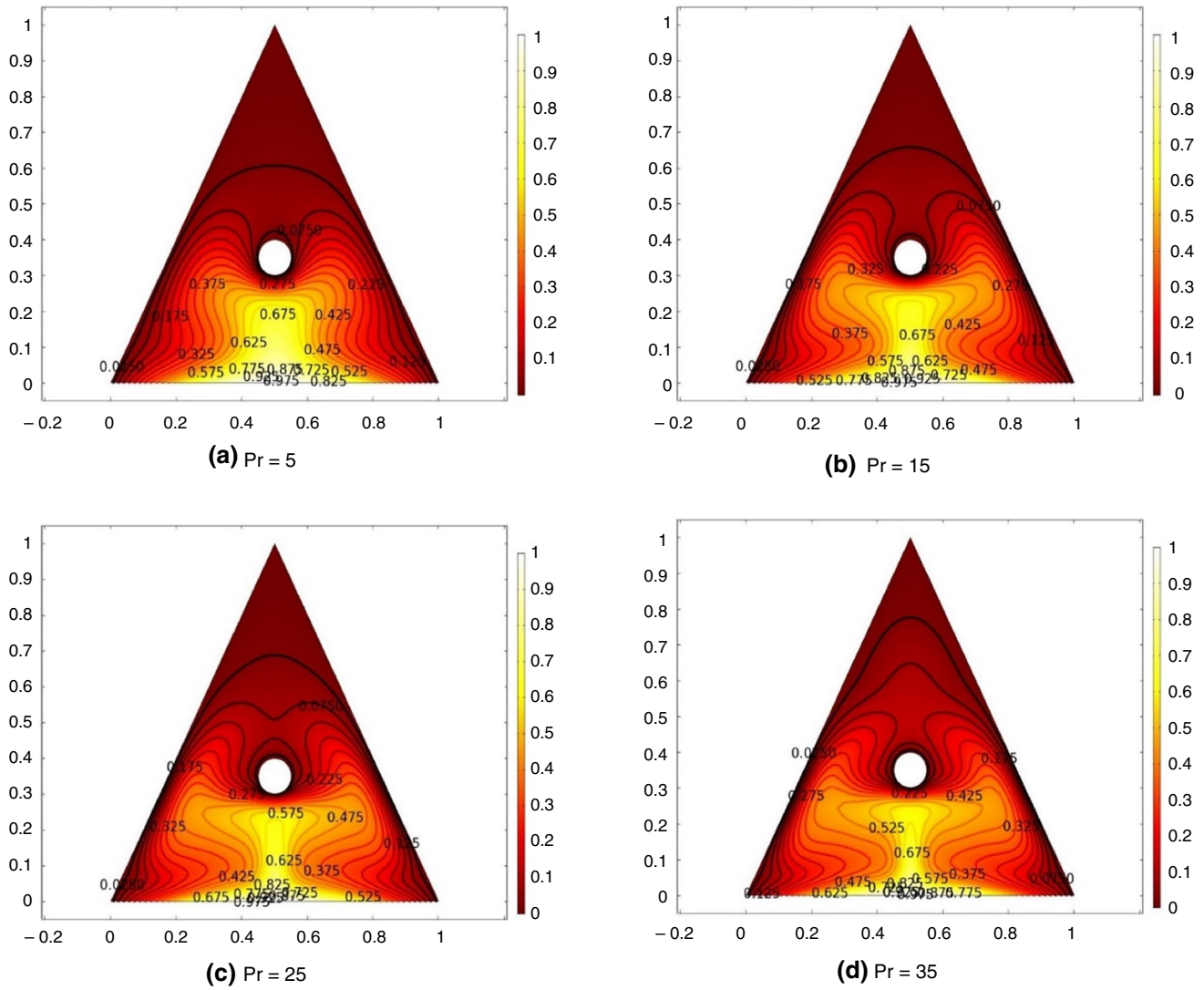

Fig. 7 Variation in thermal profile against (Pr) at Da = 0.00001

Table 2 Kinetic energy for (n) at Da = 0.0001, Ra = 1000, and Pr = 15

Power-law index (n)	Kinetic Energy (K.E)		
	$x = 0.3$	$x = 0.5$	$x = 0.8$
0.5	0.0044182	0.0016307	0.0061103
1	0.0012249	0.00042084	0.0017637
1.5	0.00084214	0.00029093	0.0012133

number shows a wide range of values for different combinations of suggestion parameters.

Figure 10 shows a line graph that displays the variation in kinetic energy (K.E.) at different Darcy numbers (Da) with an exponent (n) of 0.5. The graph shows the relationship between fluid dynamics and porous media by displaying the variation in kinetic energy across a range of Da values.

Comparison of heat transfer between different geometries

Figure 11 focuses to compare heat transfer of various geometry. The momentum profiles, which show how momentum varies within the system under these specific conditions, provide significant insight into the fluid

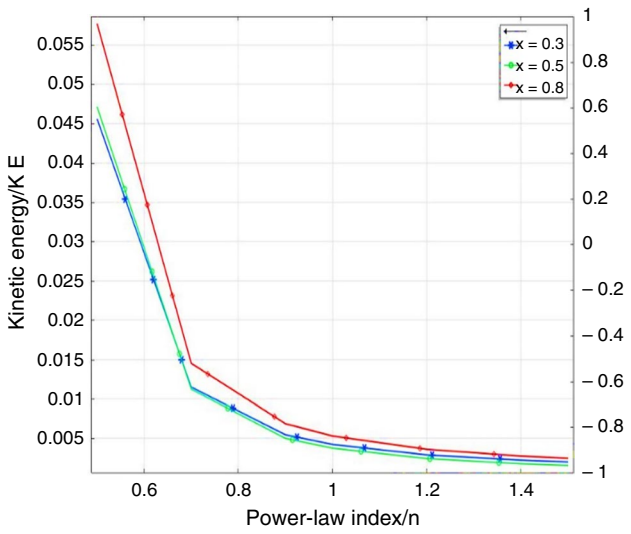

Fig. 8 Line graph of K.E. at various (n) at Da = 0.00001

Table 3 Kinetic energy for (Ra) at Da = 0.0001, n = 0.5, and Pr = 15

Rayleigh number (*Ra*)	Kinetic Energy (K.E)		
	$x = 0.3$	$x = 0.5$	$x = 0.8$
1000	0.19469	0.076273	0.27374
10000	35.484	35.489	40.833
100000	683.83	1083.8	603.00

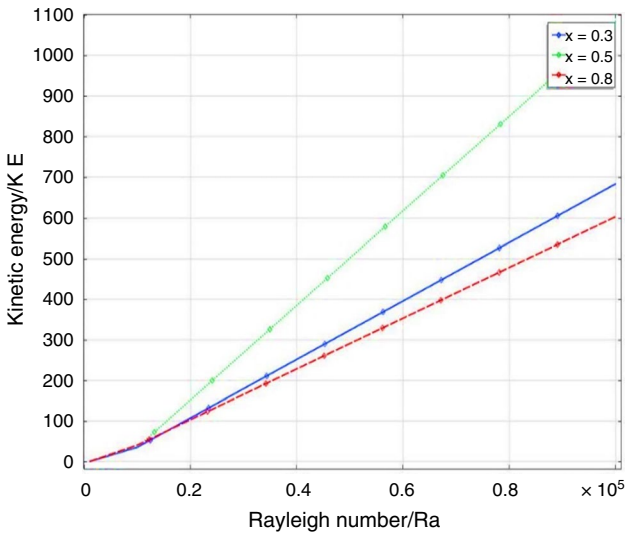

Fig. 9 Line graph of K.E. at various (Ra) at Da = 0.00001

Table 4 Kinetic energy for (Da) at n = 0.5, Ra = 1000, and Pr = 15

Darcy (*Da*)	Kinetic Energy (K.E)		
	$x = 0.3$	$x = 0.5$	$x = 0.8$
0.00001	0.0012254	0.00042100	0.0017643
0.0001	0.0018283	0.00071833	0.0025678
0.001	0.0042165	0.0037468	0.0051928

Table 5 Variation in Nusselt number against (Da), (Ra) and (Pr)

Rayleigh number (Ra)	Prandtl number (Pr)	Darcy (Da)	,,,Nusselt number (Nu)
1000			3.1688
10000	5		8.4102
100000			20.049
	15		7.0083
100	25		7.9518
	35		8.6671
		0.00001	2.9281
100	5	0.0001	3.0950
		0.001	5.0730

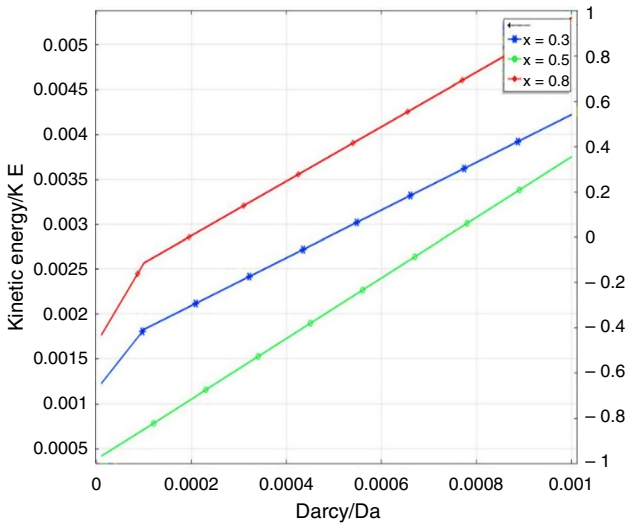

Fig. 10 Line graph of K.E. at various (Da) at n = 0.5

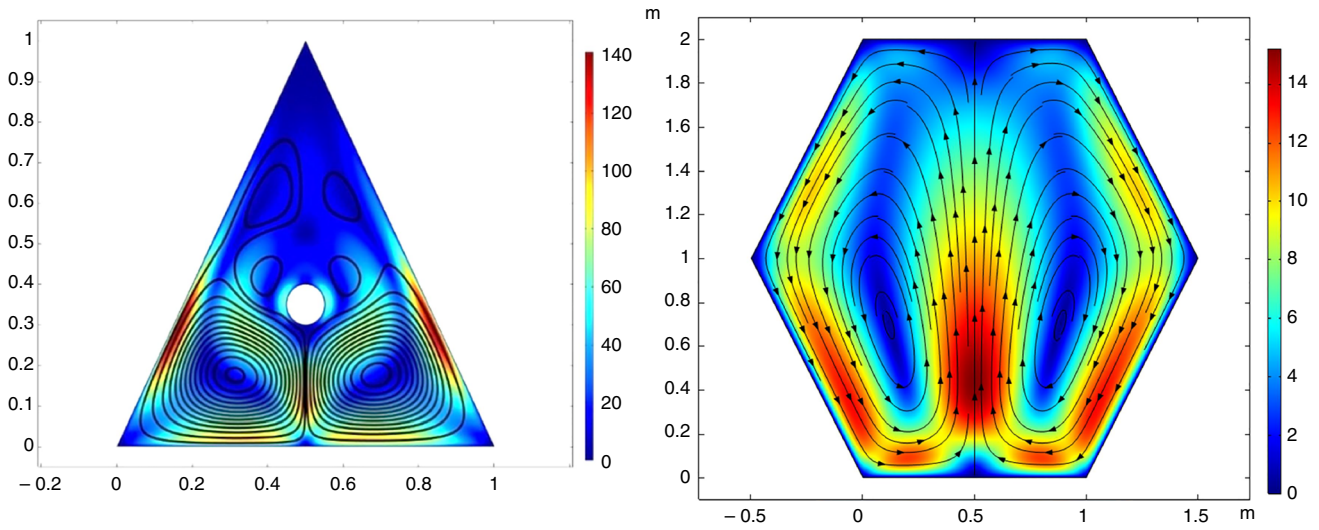

Fig. 11 Momentum profiles at Da = 0.0001, Ra = 1000, n = 0.5 and Pr = 15

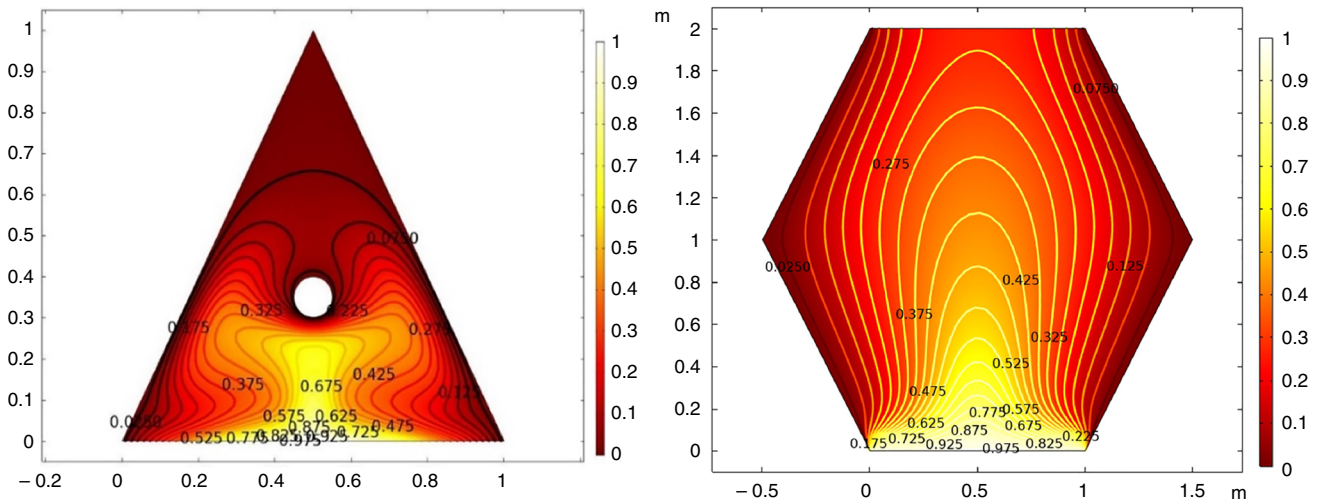

Fig. 12 Thermal profile at Da = 0.0001, Ra = 1000, n = 0.5 and Pr = 15

dynamics and heat transmission properties across a range of geometric shapes in the above figures.

Figure 12 presents of the comparison is heat transfer between two different geometries. The temperature profile provides more than just an overview of the system temperature distribution; it also clarifies the features of heat transfer and highlights the differences between the different geometries.

Conclusions

This paper investigates power-law fluid flow behavior in a triangular cavity using mathematical modeling of fluid rheology using partial differential equations. The employment of the finite element method, which uses both rectangular and triangular elements for domain discretization, is justified by the intrinsic complexity of the physical domain. Thermal contours, pressure, temperature distribution, and flow patterns are all thoroughly examined in the analysis. Non-uniform temperature differences and variable parameters like the Darcy effect (Da),

Rayleigh (Ra), and Prandtl (Pr) numbers are routinely taken into account. Among the important conclusions are the following: greater Rayleigh numbers provide more complex flow patterns and better velocity profiles, and they also raise heat transfer coefficients. Power-law fluid dynamics in triangular cavities is well understood thanks to the study's use of both quadrilateral and triangle elements for domain discretization.

References

1. Zhang L, Zhou Y, Zhang Y, Tian W, Qiu S, Su G. Natural convection heat transfer in corium pools: a review work of experimental studies. Prog Nucl Energy. 2015;79:167–81.
2. Canaan RE, Klein DE. A numerical investigation of natural convection heat transfer within horizontal spent-fuel assemblies. Nucl Technol. 1998;123(2):193–208.
3. Purusothaman A. Investigation of natural convection heat transfer performance of the QFN-PCB electronic module by using nanofluid for power electronics cooling applications. Adv Powder Technol. 2018;29(4):996–1004.
4. Bhowmik H, Tou KW. Experimental study of transient natural convection heat transfer from simulated electronic chips. Exp Thermal Fluid Sci. 2005;29(4):485–92.
5. Hanreich G, Nicolics J. Measuring the natural convective heat transfer coefficient at the surface of electronic components. In *IMTC 2001. Proceedings of the 18th IEEE Instrumentation and Measurement Technology Conference. Rediscovering Measurement in the Age of Informatics* 2001; *(Cat. No. 01CH 37188)* (Vol. 2, pp. 1045–1050). IEEE.
6. Alilat N. Natural convective heat transfer in the air-filled interstice between inclined concentric hemispheres: application to thermoregulation in electronics. Int J Numer Meth Heat Fluid Flow. 2017;27(10):2375–84.
7. Calcagni B, Marsili F, Paroncini M. Natural convective heat transfer in square enclosures heated from below. Appl Therm Eng. 2005;25(16):2522–31.
8. Buchberg H, Catton I, Edwards DK. Natural convection in enclosed spaces—a review of application to solar energy collection 1976.
9. Ozoe H, Churchill SW. Hydrodynamic stability and natural convection in Ostwald–de Waele and Ellis fluids: The development of a numerical solution. AIChE J. 1972;18:1196–207. https://doi.org/10.1002/aic.690180617.
10. M. Kaddiri, M. Naïmi, A. Raji, M. Hasnaoui, Rayleigh Benard convection of non-Newtonian power-law fluids with temperature-dependent viscosity, ISRN Thermodynamics, 2012; 614712. https://doi.org/10.5402/2012/614712.
11. Kim GB, Hyun JM, Kwak HS. Transient buoyant convection of a power-law non-Newtonian fluid in an enclosure. Int J Heat Mass Transf. 2003;46:3605–17. https://doi.org/10.1016/S0017-9310(03)00149-2.
12. Beckermann C, Ramadhyani S, Viskanta R. Natural convection flow and heat transfer between a fluid layer and a porous layer inside a rectangular enclosure 1987.
13. Murthy PVSN, Kumar BR, Singh P. Natural convection heat transfer from a horizontal wavy surface in a porous enclosure. Numer Heat Transf Part A Appl. 1997;31(2):207–21.
14. Khanafer K, Al-Azmi B, Marafie A, Pop I. Non-Darcian effects on natural convection heat transfer in a wavy porous enclosure. Int J Heat Mass Transf. 2009;52(7–8):1887–96.
15. Zahmatkesh I. On the importance of thermal boundary conditions in heat transfer and entropy generation for natural convection inside a porous enclosure. Int J Therm Sci. 2008;47(3):339–46.
16. Muhammad T, Waqas H, Khan SA, et al. Significance of nonlinear thermal radiation in 3D Eyring-Powell nanofluid flow with Arrhenius activation energy. J Therm Anal Calorim. 2021;143:929–44.
17. Akbar NS, Muhammad T. Physical aspects of electro osmotically interactive Cilia propulsion on symmetric plus asymmetric conduit flow of couple stress fluid with thermal radiation and heat transfer. Sci Rep. 2023;13:18491.
18. Afzal S, Qayyum M, Akgül A, Hassan AM. Heat transfer enhancement in engine oil based hybrid nanofluid through combustive engines: an entropy optimization approach. Case Stud Thermal Eng. 2023;52:103803.
19. Al Baidani MM, Mishra NK, Alam MM, Eldin SM, AL-Zahrani AA, Akgul A. Numerical analysis of magneto-radiated annular fin natural-convective heat transfer performance using advanced ternary nanofluid considering shape factors with heating source. Case Stud Thermal Eng. 2023;44:102825.